Journal of Marine Research, 50, 99–124, 1992

A thermocline model for ocean-climate studies

by Sheng Zhang,[1] Charles A. Lin[1,2] and Richard J. Greatbatch[3]

ABSTRACT

A 3-dimensional planetary geostrophic (PG) ocean general circulation model in spherical coordinates is formulated to examine the thermocline structure and thermohaline circulation of an idealized ocean basin. The model equations consist of full prognostic temperature and salinity equations and diagnostic momentum equations. A simple linear friction is used to close the barotropic circulation at the western boundary. An extensive sensitivity study is conducted with different model parameters and processes. The results are also compared with those obtained using the Bryan-Cox primitive equation model.

For the steady state case, the PG model can reproduce the primitive equation model results, and displays a similar sensitivity for a variety of model parameters, but with much lower computational cost. With higher vertical diffusivity and lower horizontal resolution than primitive equation models, the PG model simulates comparable currents and thermocline depth. This difference is attributed to the large horizontal eddy viscosity used in primitive equation models, but absent in the PG model formulation. The model also illustrates the crucial role of convective overturning in providing a source of cold, dense water at depth. Implications of these results to 2-dimensional zonally averaged models are discussed. In particular, we show that parameterizations used in zonally averaged models to relate the east-west pressure difference to the north-south pressure gradient are not valid when convective overturning is turned off. Finally, the model can be used to efficiently investigate time-dependent transient problems of interest in climate studies, such as the effect of seasonally varying surface forcings, without the need to use asynchronous time-stepping techniques.

1. Introduction

In contrast with the atmosphere, there is a large scale separation in the ocean between the internal Rossby radius of deformation (≈ 50 km) and the general circulation scale (≈ 1000 km). This suggests that the dominant physics governing the large scale ocean circulation may be reduced to the planetary geostrophic (PG) system, also known as the thermocline equations in the oceanic context (Robinson

1. Department of Meteorology and Centre for Climate and Global Change Studies, McGill University, Montreal, Quebec, Canada.

2. On leave (1991–92) at Laboratoire de Meteorologie Dynamique, Ecole Normale Superieure, Paris, France.

3. Department of Physics, Memorial University of Newfoundland, St. John's, Newfoundland, Canada, A18 3XZ.

and Stommel, 1959). At its core is the use of the geostrophic relation with variable Coriolis parameter as the momentum equations. The well known Sverdrup equation is a simple application of the system.

The PG system consists of the full temperature and salinity equations and diagnostic momentum equations in which the local time derivative and nonlinear advection terms are neglected. The resulting geostrophic balance is a very good approximation for scales larger than the Rossby radius of deformation. This approximation can be justified by scale analysis, using the time (1 month and longer) and space (larger than 500 km) scales of interest in climate studies, as well as by wave property analysis (Hasselmann, 1982). The dominant wave which exists in this space-time domain is the long baroclinic Rossby wave. The latter is also the only wave in the PG model, and it is necessary for the adjustment of the density field to equilibrium. There is no doubt that this approximation is a good one in the interior ocean, but it can be problematic in the tropics and near boundaries. Nevertheless the results we shall present suggest that these difficulties are often less important than others associated with coarse resolution models, e.g., subgrid scale eddy parameterization.

Primitive equation model results exhibit a large scale circulation which is quite geostrophic. For example, the results of Bryan and Lewis (1979) show that, under a wide range of closure parameters, the ratio of available potential energy and kinetic energy remain nearly constant. This result was interpreted as being due to geostrophy. This suggests that a model formulated using PG dynamics should be capable of reproducing primitive equation model results, a point that we investigate in this paper. The principal advantage of such a model is that the time step is limited only by the ocean current speed, and is thus larger than that allowed by primitive equation dynamics. The computational cost is thus much lower, which in turn allows for a large number of model simulations to examine parameter sensitivity. As noted already, this efficiency of the PG model is due to the filtering of time and space scales to those of interest to climate. It is thus an ideal model for use in climate studies.

When seeking only steady state solutions, the use of "distorted physics" with primitive equation models can also significantly reduce computational needs (Bryan, 1984). Larger time steps are used in the equations which govern slowly varying processes, thus permitting an acceleration in the time marching procedure. The equilibrium state thus reached is not distorted; but the transient evolution to equilibrium can be distorted considerably. The removal of distorted physics, such as a switch from asynchronous integration to synchronous integration, may render unstable a previously stable steady state obtained using distorted physics and mixed upper boundary conditions (Weaver and Sarachik, 1991). In contrast, the PG system can be used to examine not only the equilibrium state, but also the transient behavior with the same time step and efficiency. This is of great interest to the study of interannual variability of the climate system.

The PG system is a well accepted approximation for the large scale ocean circulation. Its use for the modelling of the global ocean circulation goes back to Veronis (1973). However, it is only recently that it has been used in numerical modelling; notably the pioneering work of the group at the Max Planck Institute für Meteorologie in Hamburg, Germany. (Hasselmann, 1982; Maier-Reimer and Hasselmann, 1987; Bacastow and Maier-Reimer, 1990). This general circulation model uses a time step of 1 month, made possible by the use of an implicit time integration scheme. The simulation of water properties is good, and the model has also been used to study the global carbon cycle. Other models using the PG system have appeared since then (e.g., Killworth, 1985; Colin de Verdière, 1988; 1989). These models use β-plane box geometry with Cartesian coordinates, and idealized forcing. The sensitivity to the model parameters, especially the closure terms, have been examined in these studies. Recently, Greatbatch and Goulding (1992) have described an application of the same idea to shelf circulation modelling.

The present model is an extension of the 2-level model of Killworth (1985) on a β-plane to a multi-level model on the sphere. Unlike the model proposed by Hasselmann (1982), we do not include special boundary layers at the equator or at coasts. Also, unlike Colin de Verdière (1988), horizontal mixing of momentum is explicitly excluded. Friction is provided through a simple, linear Rayleigh friction in the momentum equations. In this respect, the papers of Salmon (1986, 1990) are highly relevant to our study. It is shown in Salmon (1986) that replacing the traditional Laplacian viscosity and thermal diffusivity by a linear-decay friction and heat diffusion leads to solutions of the linearized equations of motion that display all the physically important features of the standard model. In the later paper (Salmon, 1990), he extends this work by including a non-linear density equation. However, in order to satisfy a "no normal flow" condition at the coastal boundaries, it is necessary to relax the hydrostatic approximation and include Rayleigh friction in the vertical as well as the horizontal momentum equations. In this paper, we do not include these non-hydrostatic effects. Rather, our concern is to develop a computationally efficient, coarse resolution model that can be used for climate studies. It should be noted, however, that if the grid resolution of our model were progressively refined, then it is unlikely our model would give a convergent solution. We shall return to this point in Section 2 when we discuss boundary conditions for the model.

In order to illustrate the behavior of our model, we consider an idealized, box geometry on the sphere, with a horizontal resolution of $2° \times 2°$ latitude/longitude, and either 10 or 14 vertical levels. In general, any horizontal/vertical resolution or model geometry could be used. Numerical experiments are conducted to test the model sensitivity to various processes and parameters. A detailed comparison with the Bryan-Cox primitive equation model is also performed.

The rest of the paper is organized as follows. Section 2 is the model formulation, and the comparison with primitive equation model results are shown in Section 3.

Numerical experiments on process sensitivity studies and the role of convective overturning are described in Sections 4 and 5 respectively. The conclusions are presented in the final section.

2. Model formulation

The model used in this study is a multilevel numerical model of the PG system in spherical coordinates. As noted earlier, the major difference between the PG and primitive equation models is the omission of the time derivative in the momentum equations. Fast waves are filtered by this diagnostic approximation, thus allowing the use of a larger time step. We also omit the nonlinear advection terms and use a simple linear friction to close the circulation at the western boundary. Weaver and Sarachik (1991) found that the former played no role in their calculations using a primitive equation model and could thus be safely omitted. The model equations with the Boussinessq approximation are shown below.

$$f\,\mathbf{k}\times\mathbf{V} = -\rho_0^{-1}\nabla p + (\tau_s/\rho_0 H_1)G(z) - \gamma(\mathbf{V}^+ + \epsilon_1\mathbf{V}') \tag{1}$$

$$p_z = -\rho g \tag{2}$$

$$w_z + \nabla\cdot\mathbf{V} = 0 \tag{3}$$

$$Q_t + \nabla\cdot(\mathbf{V}Q) + (wQ)_z = A_h\nabla^2 Q + A_v Q_{zz} + F + CON \tag{4}$$

$$\rho = \rho(S, T) = 0.77S - 0.072T\,(1 + 0.072T). \tag{5}$$

The notation used is standard. Dependent variables are the horizontal velocity ($\mathbf{V}$), vertical velocity (w), pressure (p), density (ρ), salinity (S in parts per thousand), temperature (T in degrees Celsius); ρ_0 is a reference density. The horizontal velocity field is made up of the barotropic ($\mathbf{V}^+$) and baroclinic ($\mathbf{V}'$) components. Independent variables are time (t), longitude, latitude and height (z). The remaining variables are the Coriolis parameter (f), wind stress (τ_s), depth of top model level (H_1), frictional dissipation coefficient (γ), temperature, salinity, density or radioactively decaying tracer (Q), horizontal (A_h) and vertical (A_v) eddy diffusivity, surface forcing for tracer field (F), and convective adjustment (CON). The vertical structure function $G(z)$ for the surface forcing is unity in the top model level, which is taken to be the mixed layer, and vanishes elsewhere. Eqs. (1)–(5) are the horizontal momentum, hydrostatic, continuity, tracer conservation, and state equations respectively. The momentum equation is geostrophic except for wind and a simple linear friction. The frictional term contains a multiplier ϵ_1 which takes on the value of either 0 or 1. There are no frictional effects in the baroclinic component when $\epsilon_1 = 0$. Most of the experiments carried out in this study have $\epsilon_1 = 0$. This point is discussed further when we describe the boundary conditions.

We may form the vorticity equation from the horizontal equations of motion, which in turn can be separated into the barotropic ($\mathbf{V}^+$) and baroclinic ($\mathbf{V}'$) compo-

nents. For future reference, we show below the barotropic vorticity equation, and the baroclinic momentum equation.

$$\beta \mathbf{V}^{+} = (\rho_0 H)^{-1}\mathbf{k} \cdot (\nabla x \boldsymbol{\tau}_s) - \gamma \mathbf{k} \cdot (\nabla x \mathbf{V}^{+}) \tag{6}$$

$$f\,\mathbf{k}x\mathbf{V}' = -\epsilon_2 \rho_0^{-1} \nabla(p - p^{+}) + (\tau_s/\rho_0)[H_1^{-1}G(z) - H^{-1}] - \epsilon_1 \gamma \mathbf{V}'. \tag{7}$$

β and H = 4000 m denote the meridional gradient of the Coriolis parameter and the total ocean depth respectively; γ is the dissipative coefficient and has the value $1.04 \times 10^{-6}\text{s}^{-1}$ in all the experiments; p^{+} is the barotropic pressure field. The multiplier ϵ_2 again takes on the value of either 0 or 1; $\epsilon_2 = 0$ corresponds to the case in which the baroclinic pressure gradient is set to zero (see later discussion). (6) is the same equation as considered by Stommel (1948) in his famous paper.

We now turn to the surface forcing (F) and convection (C) terms in the tracer equation (4). The former is given by a Newtonian relaxation of the top layer tracer value (Q_1) to a prescribed equivalent atmospheric value (Q_a) (Haney, 1971).

$$F = -D(Q_a - Q_1)G(z). \tag{8}$$

The relaxation time scale is given by D^{-1}. A radioactive decaying tracer equation can be included, by adding the decay term $-\lambda Q$ to the right-hand side of the appropriate tracer equation (4); λ is the decay constant. Convective adjustment (C) takes place when the density in any control volume exceeds the value below it, and is such as to guarantee a stable profile.

The equation of state (5) includes quadratic terms in temperature and linear terms in salinity, with coefficients similar to those of Bryan and Cox (1972). This approximates the different effects of temperature and salinity on density. No depth dependence is assumed; i.e., compressibility effects are ignored in this study.

The finite difference scheme used in the model is the Arakawa C-grid. The scheme uses the control volume concept and possesses two invariants: the first and second moments of the tracer distribution for the advection operator, and the first moment for diffusion. The numerical procedure is as follows. Since the model is flat-bottomed and is forced by a steady wind stress, the barotropic velocity is time independent and needs only be computed once, using Eq. (6). The baroclinic velocity is then obtained from the density field using Eqs. (2), (3), (5), and (7). After combining with the barotropic velocity, the total velocity field is used to advance the tracer field using Eq. (4). This then completes the integration for one time step. The time integration is performed using the leap-frog scheme, with the Matsuno scheme used in the initial step. To prevent time splitting, the tracer field is averaged over 3 adjacent time steps for every 32 time steps of the integration.

In all the experiments described in this paper, we follow Killworth (1985) and use "no slip" conditions on the coastal boundaries. The use of the "no slip" condition facilitates comparison with primitive equation models which also use a "no slip" condition (Section 3). Killworth noted that substituting the "no slip" condition with

one of only "no normal flow" did not significantly change his model solutions. This is also true of the solutions we present in this paper. However, as discussed by Killworth, an unstable computational mode can be excited along the boundaries if the time step is too large. He gives a criterion that must be satisfied in order to prevent excitation of this instability. In all the experiments we describe, our grid spacing is sufficiently large that this is never a serious restriction. Killworth notes, however, that the criterion becomes more stringent as the grid spacing is reduced. This is an indication that our model equations lack some of the physics necessary to satisfy the imposed boundary conditions. (This is also indicated by the apparent interchangability of the "no slip" and "no normal flow" boundary conditions.) Indeed, although a "no-slip" boundary condition is easily implemented numerically, it is not strictly valid unless horizontal (Laplacian) mixing of momentum is included in the momentum equations. It might be thought that replacing this horizontal mixing by a linear, Rayleigh friction (as we do in some of our experiments) would allow the "no slip" condition to be replaced by one of "no normal flow." However, as discussed by Salmon (1986, 1990), to satisfy a "no normal flow" condition, the hydrostatic approximation must be relaxed and the Rayleigh friction included in the vertical as well as the horizontal momentum equations. The corresponding boundary layer is only a few kilometers wide and would certainly not be resolved in a course resolution model such as ours. Indeed to use a grid spacing sufficiently small to resolve this boundary layer would severely limit the computational advantage of our model by requiring the use of a correspondingly small time step. As it happens, in our model, not only do we make the hydrostatic approximation, but in most of the experiments we also set the Rayleigh friction to zero for the baroclinic part of the flow (i.e. we put $\epsilon_1 = 0$ in (7)). It follows that successive refinement of our model grid is unlikely to lead to a convergent solution without including some additional physics. One final point to note is that if the depth goes to zero at the coast (as it would if variable bottom topography is used with the model) then the need for a non-hydrostatic model is eliminated and a "no normal flow condition" can then be satisfied at the coast as long as a linear Rayleigh friction is used in the baroclinic as well as the barotropic parts of the motion (i.e. as long as $\epsilon_1 = 1$ in (7)). For another discussion of boundary conditions in the context of the thermocline equations, the reader is referred to Killworth (1983).

As noted above, in most of our experiments the friction in the baroclinic momentum equation (7) is set to zero. We shall show in Section 4 that including this friction has the effect of reducing the velocities computed by the model. It does not, however, seem to change the basic structure of the solution and, in fact, in the experiments in Section 3, where we compare our model with results from the Bryan/Cox primitive equation model (Cox and Bryan, 1984; Cox, 1985), the baroclinic friction is set to zero. This seems to contradict Veronis (1973) who noted the importance of friction in the dynamics of separated western boundary currents. Since separated boundary

Table 1. The depths of the bottom of each level, for the 10- and 14-level versions of the model.

Layer	10-level	14-level
1	68 m	28 m
2	164	65
3	300	114
4	492	179
5	764	265
6	1148	378
7	1692	528
8	2460	726
9	3230	989
10	4000	1336
11	—	1796
12	—	2404
13	—	3202
14	—	4000

currents are a feature of our solutions (see for example Figs. 6 and 9), it is not clear why setting the baroclinic friction to zero works so well.

The model geometry used in this paper is a latitude/longitude box on the sphere of size similar to the North Atlantic, with slightly different domain sizes for two different sets of experiments. The first domain has meridional boundaries at the equator and 65N, and zonal boundaries at 0 and 60E, and is used in Section 3. The second, used in Sections 4 and 5, is bounded by the latitudes 10 and 60N, and longitudes 0 and 50E. In both cases, 27 grid points are used in each horizontal direction, giving a horizontal resolution of about $2° \times 2°$ in latitude/longitude. The total model depth of 4000 m is resolved by either 10 or 14 levels in the vertical, depending on the particular experiment. The vertical structure is summarized in Table 1. The time step used is 2–5 days, with the smaller time step used for experiments which include the equator (the smaller time step is required to overcome the boundary instability noted by Killworth, 1985). A 1000-year integration requires approximately 2 hours cpu time on an IBM RISC/6000 workstation for the version of the model with the smaller domain. All the model experiments we shall describe have been run to a statistically steady state with no trend in basin mean quantities.

3. Comparison with primitive equation (PE) model results

In this section, we compare the results of our PG model with several studies which use a PE model (Cox and Bryan, 1984; Cox, 1985; hereafter referred to as CB and CX respectively). We also perform a sensitivity study of model parameters, and compare the results with the PE model results of Bryan (1987). The purpose of this part of the study is to show that the PG model is capable of reproducing most of the PE model results, with much less computational cost.

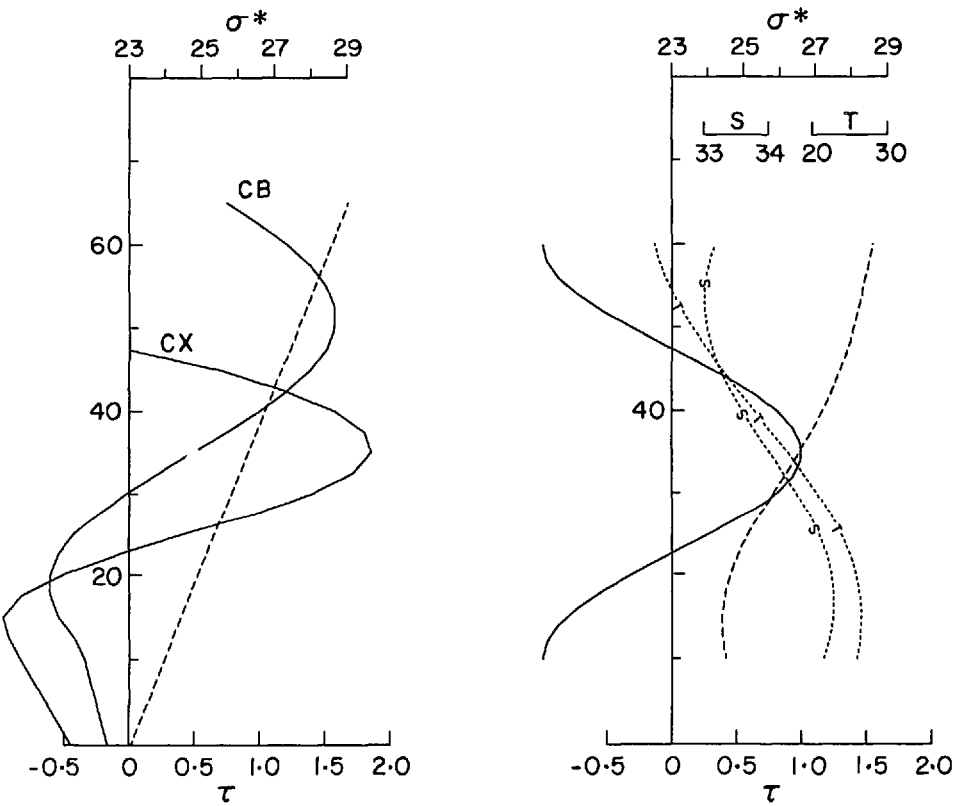

Figure 1. The latitudinal (ϕ, °N) distributions of the surface wind stress (τ, dynes/cm^2; solid), and buoyancy (σ^*, σ-units; dashed) boundary conditions. (a) Used in Section 3; CB and CX denote Cox and Bryan (1984) and Cox (1985) respectively. (b) Used in Sections 4 and 5. Curves labelled S and T denote respectively the salinity and temperature contributions to the buoyancy forcing.

CB and CX simulated the thermocline with coarse horizontal resolution, using the widely distributed Bryan-Cox PE model (Bryan, 1969; Cox, 1984). It should be noted that CB and CX integrated the equations of motion for an incompressible ocean, working with density only and not integrating separate equations for temperature and salinity. In this section we follow these authors in doing likewise. We perform two simulations with identical surface wind and buoyancy forcings as these studies. The surface wind stress and equivalent atmospheric buoyancy (see Eq. (8)) are independent of longitude, and are displayed in Figure 1a, adapted from CB and CX. A summary of the model parameters used in the experiments in this study is shown in Table 2. Both CB and CX use a horizontal resolution of 1° × 1°, while we use 2° × 2°. The vertical resolution is also higher in the PE studies (15 and 18 levels in CB and CX respectively), than in ours (10 and 14 levels). Our results are more sensitive to the vertical resolution in the CX case compared to the CB case, thus more levels are used

Table 2. A summary of the model parameters used in the numerical experiments.

Domain	$\Delta\lambda, \Delta\phi$	Level	A_h	A_v	D^{-1}
Section 3					
CB 0–65N, 0–60E	1° × 1°	15	1×10^7 cm^2 s^{-1}	0.3 cm^2 s^{-1}	10 d
PG (as CB)	2° × 2°	10	2	0.4	50
CX 0–65N, 0–60E	1° × 1°	18	1	0.3	50
PG (as CX)	2° × 2°	14	1.5	0.4	32
Sections 4, 5					
10–60N, 0–50E	2° × 2°	10	2.5	0.75	50

in the former simulation; all other experiments in this study use 10 levels. Table 1 contains a description of the level structure. The basin configuration is identical, except we do not have the small continental shelf along the western wall north of 35° used in CX. We need to use a slightly larger vertical diffusivity in order to get similar results as CB and CX.

Three meridional cross sections in the western, central and eastern parts of the basin from CB (their Figures 3, 4 and 5) and from the PG model are shown in Figures 2 and 3 respectively. We see the thermocline structures and the circulation patterns are quite similar. The simulated velocities in both models are of comparable magnitudes. This agreement obtains in spite of the lower horizontal resolution used in the PG model, due probably to the absence of friction in the baroclinic momentum equations in the PG model (the PG experiments in this section all have $\epsilon_1 = 0$ in (1)).

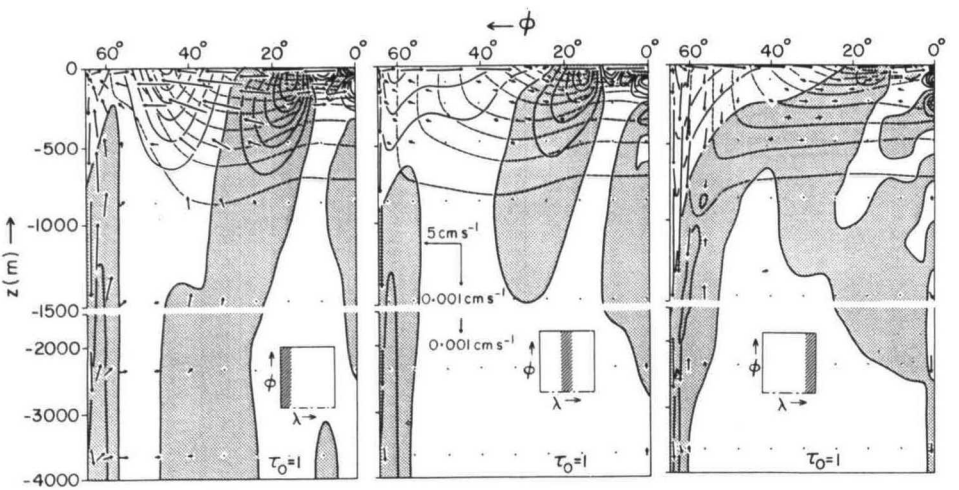

Figure 2. Meridional sections, averaged zonally across the western, central, and eastern 12° of the basin (shown by hatching in the inset), for the primitive equation model of CB. The (v, w) velocity components are shown by vectors, and u is contoured by solid lines at an interval of 1 cm/s, with stippling indicating westward flow. Isopycnals are indicated by dashed lines at 0.4 σ-unit intervals.

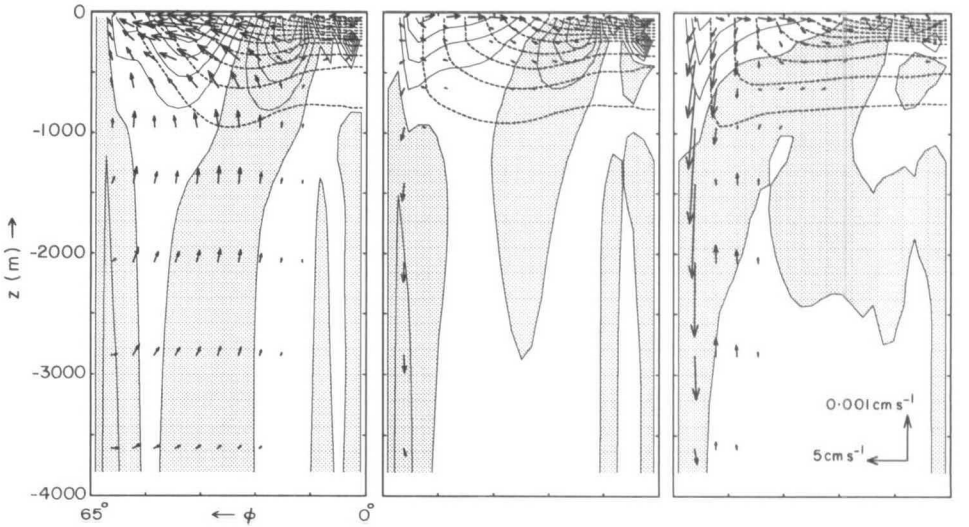

Figure 3. As Figure 2, but for the PG model.

CB did not state the amplitude of the meridional streamfunction, but the similarity of the meridional and vertical motion fields suggests that they are quite comparable in the two models.

We now turn to a comparison with the CX case. We use as diagnostics the distributions of a radioactive tracer and potential vorticity as simulated by the models. The decay constant used corresponds to tritium, with a half-life of 12.3 yrs, as in CX. Figure 4 shows the two distributions on the isopycnal surface $\sigma = 26.0$, while Figure 5 shows the vertical section averaged over the longitude band $\lambda = 24°–36°$. The corresponding figures from CX are also shown for comparison. We see that the tracer distribution is quite similar to that of CX; the homogenized, ventilation and shadow zones (Luyten *et al.*, 1983) can clearly be identified. A slightly lower value of the tracer concentration is simulated by the PG model in Figure 4. The potential vorticity distribution shows a maximum at the eastern boundary of the domain, with a tongue of low potential vorticity water extending across the basin; both these features are simulated by the PG model. We see from Figure 5 that both tracer and potential vorticity gradients are large near the $\sigma = 26.0$ surface, which in turn means that a small displacement can result in differences between the two simulations.

The vertical diffusivity used in the PG and the primitive equation models are $A_v = 0.4$ and 0.3 cm^2 s^{-1} respectively. We note that the depth of the thermocline as simulated by both models are comparable, despite the use of a larger vertical diffusivity in the PG model. This suggests that the latter would simulate a shallower thermocline for the same value of the vertical diffusivity. (Unfortunately the vertical

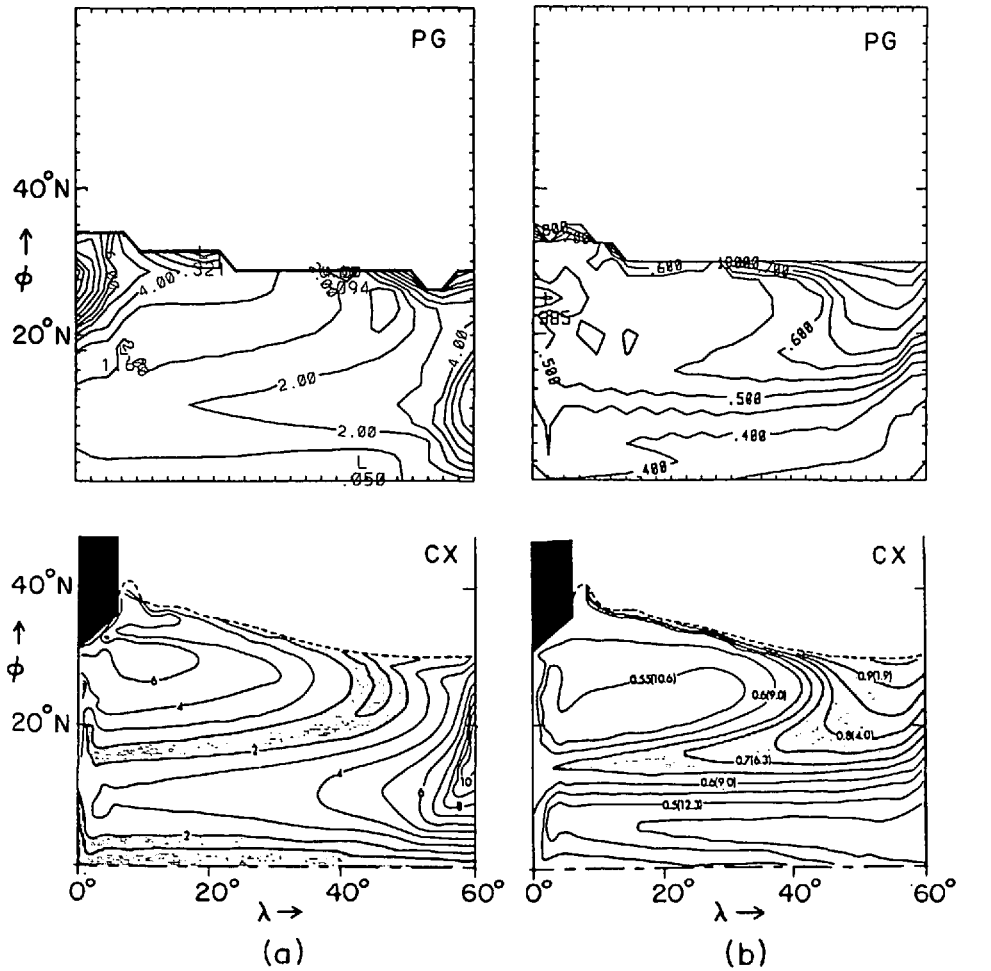

Figure 4. Quantities evaluated on the σ = 26.0 surface, from the CX and PG models. (a) Tracer concentration (time-since-ventilation in years, in parentheses for CX). (b) Potential vorticity (10^{-9} cm^{-1} s^{-1}). The continental shelf in the western basin is absent in the PG model. The data in (a) were four point averaged before plotting.

levels used by CB and CX are not given explicitly in their paper. Comparison experiments with identical vertical resolutions are required to verify this.)

The above direct comparison of the PG and PE model results shows that the PG model contains the essential physics which govern the large scale ocean circulation. Indeed, for the steady state results examined in this section, there is little difference between the two sets of governing equations, if we assume that the detailed form of the viscous terms and also the momentum advection terms do not play a major role in the dynamics of the large scale circulation.

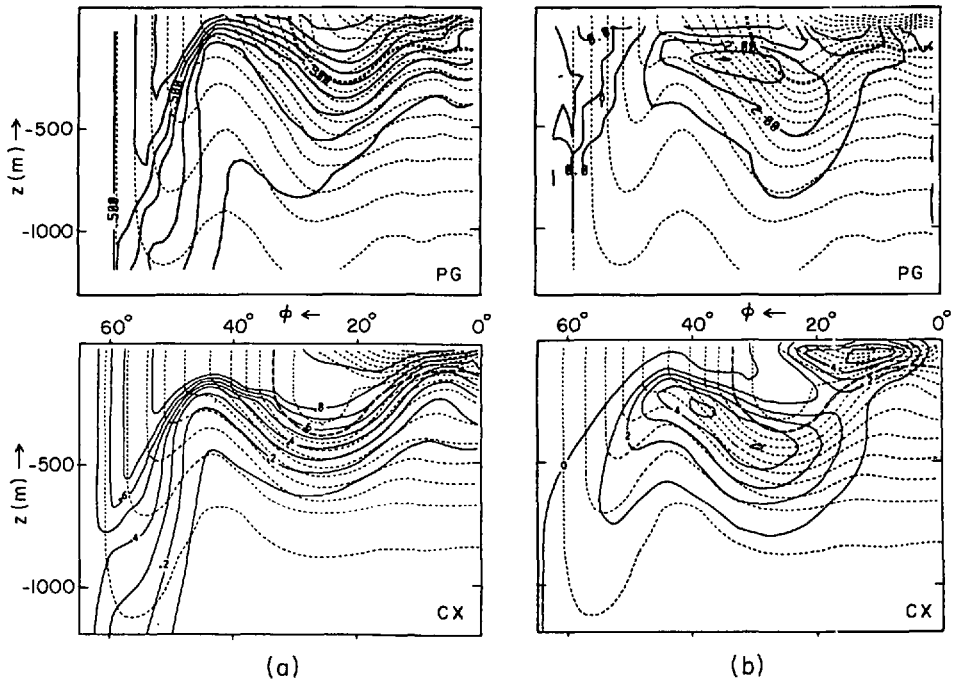

Figure 5. Quantities averaged between longitudes $\lambda = 24°$ and $\lambda = 36°$, from the CX and PG models. The dashed lines indicate isopycnals at 0.4 σ-unit intervals, with $\sigma = 26.0$ emphasized. Solid lines are contours of (a) tracer concentration; and (b) potential vorticity (10^{-9} cm^{-1} s^{-1}).

We close this section by examining the sensitivity of the model results to variation in the vertical diffusivity. Bryan (1987) has shown that the thermocline and thermohaline circulation is sensitive to variations of this parameter in a PE model. The model configuration, surface forcing and all model parameters except the vertical diffusivity remain the same as in the comparison with CB discussed earlier. We show results for three values of the vertical diffusivity $A_v = 0.1$, 0.4, 1.6 cm^2 s^{-1}. Figure 6 shows the surface density and velocity fields, and Figure 7 shows the thermocline and the meridional overturning circulation, for the various A_v values. With increasing values of the vertical diffusivity, the subtropical gyre extends to higher latitudes, the western boundary current becomes stronger, and a tongue of low density water due to the enhanced current advection develops (Fig. 6). At the same time, the thermocline deepens, especially at low latitudes (Fig. 7), and the strength of the meridional overturning circulation increases. This behavior is found by Bryan (1987) and is discussed further in Section 5. In Figure 7, each tick mark in the horizontal represents the center of a grid box. In the vertical, a tick mark denotes the bottom of a level. As the resolution is uniform in the horizontal but not in the vertical, this means that the vertical direction is distorted in the figure. This is done so that the

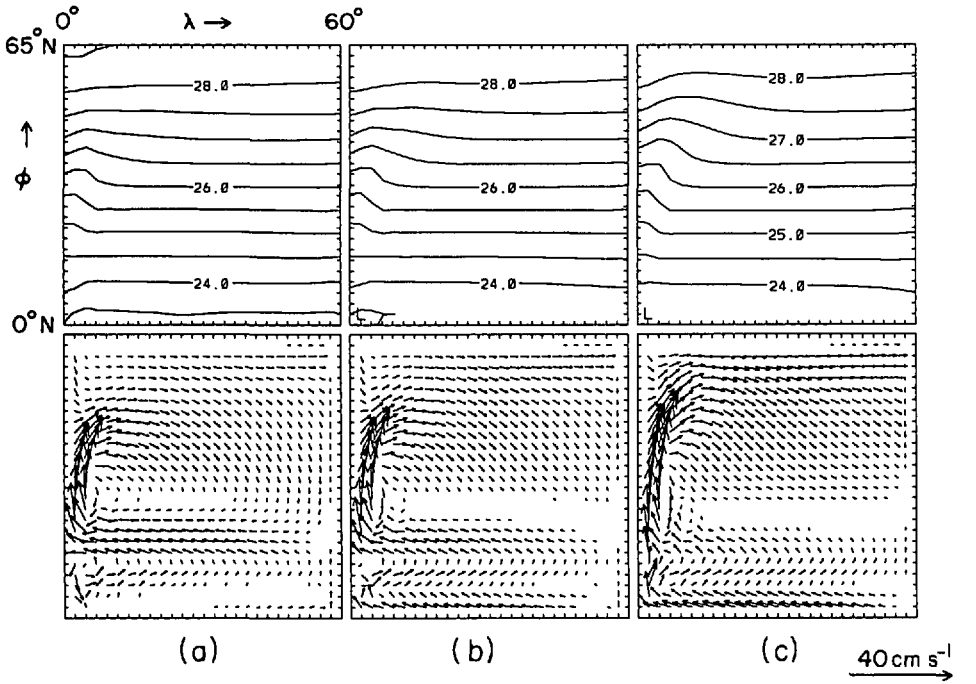

Figure 6. The horizontal distribution of quantities in the top model level, for vertical diffusivities A_v = 0.1, 0.4, and 1.6 cm^2 s^{-1}, (these are cases marked (a), (b) and (c) respectively). The top panels show the density in σ-units, while the bottom panels show the horizontal velocity vectors. The scale for the latter is indicated by the arrow in the lower right.

thermocline is more clearly visible. The position of each vertical level is given in Table 1.

Our model results also show small scale features in the meridional streamfunction in the tropical regions (Fig. 7). This phenomenon appears at low vertical diffusivities, and is probably due to inadequate vertical resolution for these values of the diffusivity (Weaver and Sarachik, 1989).

4. Process sensitivity studies with the model

In the following two sections, we examine the role of different processes in the model simulation by performing a sensitivity study with the model. The purpose is to ascertain which are the major processes that determine the thermocline structure and thermohaline circulation in the model. In particular, the roles of wind and buoyancy forcing, damping in the baroclinic component of the momentum equations, and convection will be examined in this section. As the latter process can lead to qualitative changes in the simulated circulation, we examine the role of convection more closely in Section 5.

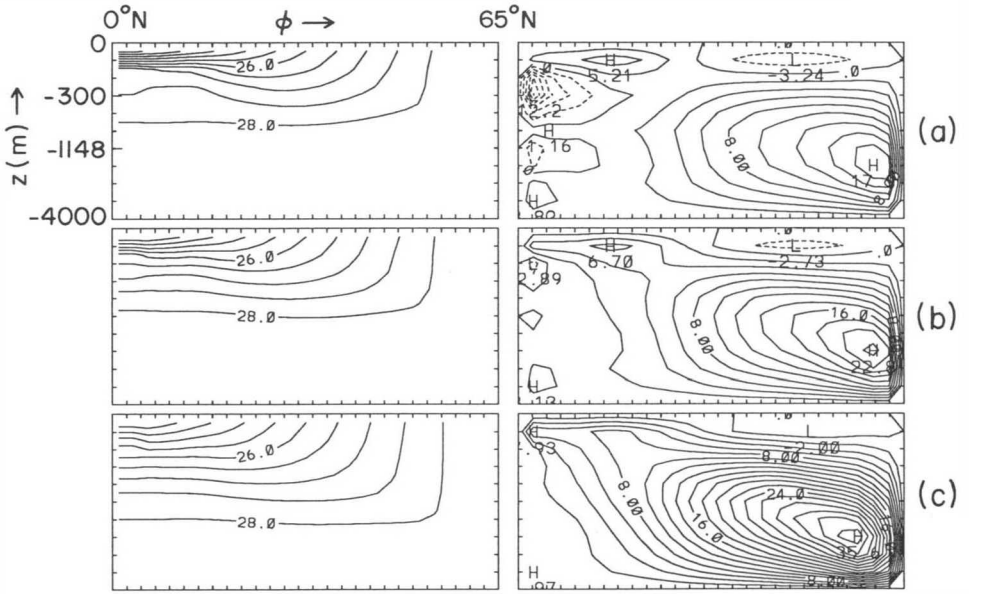

Figure 7. Basin wide zonally averaged quantities for vertical diffusivities A_v = 0.1, 0.4 and 1.6 $cm^2\ s^{-1}$, (these are cases marked (a), (b) and (c) respectively). The left panels show the potential density distribution (σ-units), and the right panels show the meridional overturning streamfunction (Sv).

For the model results described in this and the next section, the model domain is 10–60N, 10–60E, with 10 levels in the vertical. The model is forced at the surface with an idealized wind stress distribution, and Haney restoring boundary conditions (8) for both temperature and salinity. The prescribed atmospheric values in (8) are also idealized, varying in the zonal direction only. The wind, temperature and salinity surface forcing distributions are shown in Figure 1. The time scale for the surface forcing is D^{-1} = 50 days.

For our surface forcing functions shown in Figure 1(b), the simulated salinity fields are quite similar to the temperature fields, thus resulting in similar density fields as well. The effects of salinity on density is opposite to that of temperature, but is much weaker, especially at low latitudes. We thus show only the temperature field in subsequent discussion, noting that salinity effects do not result in qualitative changes in the model simulations.

The experiments conducted in this section are summarized in Table 3. The control run, case (a), has no damping in the baroclinic momentum equations, and has wind forcing as well as convective adjustment. Cases (b)–(e) examine the roles of wind forcing, buoyancy forcing, baroclinic damping, and convection in the model simulation respectively. In the wind driven case (b), the current field is determined exclusively by the wind stress, with the effect of the density field on the pressure field

Table 3. Summary of experiments conducted in Sections 4 and 5 to examine the role of different processes in the model simulation of the thermocline structure and thermohaline circulation.

Case	ϵ_1	ϵ_2	*CON*	τ_s
a. Control	0	1	yes	yes
b. Wind only	0	0	yes	yes
c. Buoyancy only	0	1	yes	no
d. Baroclinic damping	1	1	yes	yes
e. No convection	0	1	no	yes

being eliminated. For the buoyancy driven case (c), there is no barotropic velocity and the baroclinic motion field is thus geostrophic. Case (d) includes damping in the baroclinic momentum equation (7), while case (e) has no convective adjustment.

Figures 8–10 show various features of the simulated circulation for the different cases. The thermocline (zonally averaged temperature structure), and thermohaline circulation (zonally averaged overturning circulation) are shown in Figure 8. The horizontal circulations at the top level (34 m) and level 8 (2076 m) are shown in Figures 9 and 10.

As the eddy diffusivities have the same values for these experiments ($A_h = 2.5 \times 10^7$ cm^2 s^{-1}, $A_v = 0.75$ cm^2 s^{-1}), any differences in the flow features among the cases examined reflect directly the role of the individual process involved. The control run shows a typical thermocline structure with upwelling at the equatorial regions, and a thermohaline circulation with downwelling at the high latitudes (Fig. 8a). The mass transport by the latter is about 17 Sv. The horizontal surface flow shows a 2-gyre structure in response to the wind forcing, with the surface western boundary current reaching a maximum magnitude of about 30 cm s^{-1} (Fig. 9a). There are also weaker return western boundary currents at lower levels (Fig. 10a).

Comparing the different thermoclines in Figure 8 for the various cases, we see that cases (a), (c) and (d) yield similar results. The wind driven case (b) shows a much deeper thermocline, while case (e) with no convection shows a statically unstable thermocline forming at high latitudes. We will examine each of these cases in turn. In the wind driven case (b), downward Ekman pumping at the low latitudes deepens the thermocline to the bottom of the ocean. The only counteracting mechanism is convective overturning, which provides cold bottom water and maintains the sense of the thermocline at low latitudes. The response changes dramatically when convection is eliminated in case (e), the thermocline now forms at the high latitudes. Bottom water is now formed at low latitudes where the downward Ekman pumping is maximum, with a temperature of about 24°C. Since horizontal diffusion is stronger in its effect than vertical diffusion, the warm bottom water spreads across the entire ocean basin. A thermocline thus forms at the high latitudes with cold water at the surface. The southward Ekman drift at mid-latitudes is not required in this thermocline reversal, it simply extends the reversed thermocline to lower latitudes. The

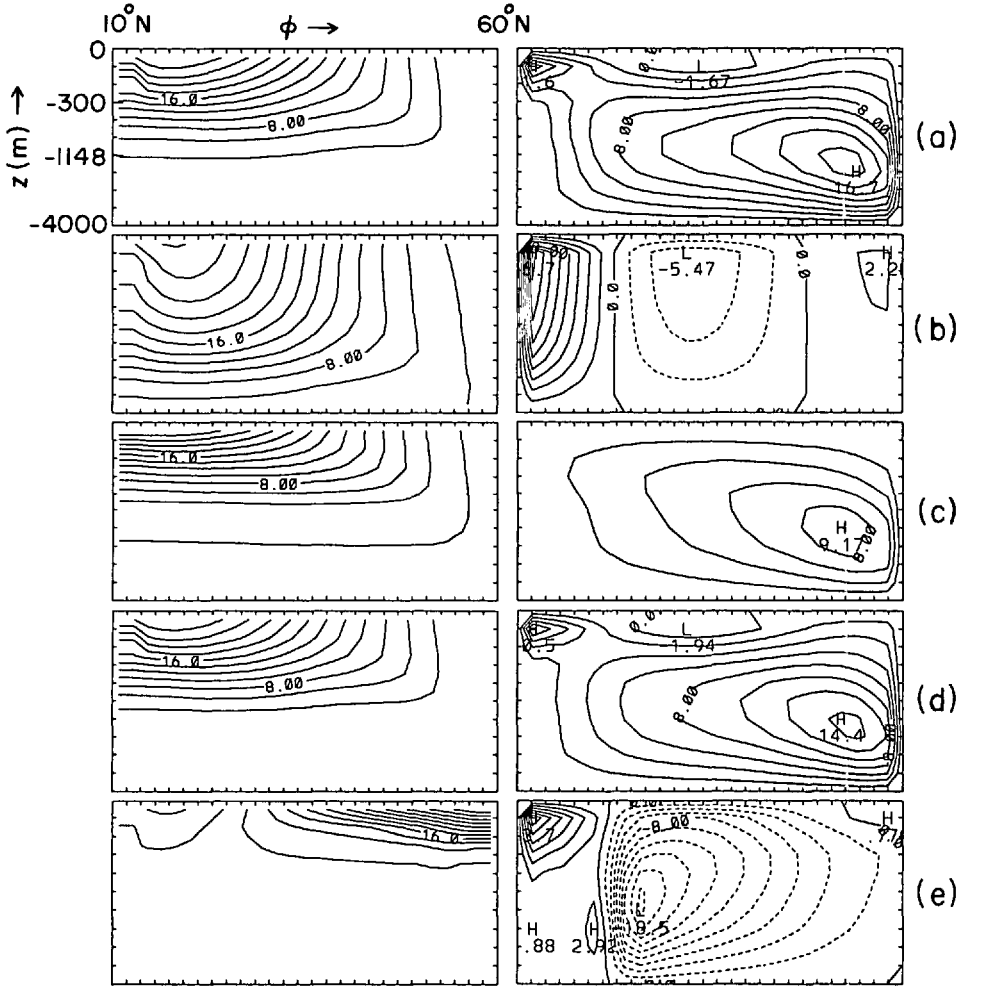

Figure 8. Basin wide zonally averaged quantities for cases (a)–(e) of Table 3. The left panels show the temperature distribution (°C), and the right panels show the meridional overturning streamfunction (Sv).

sense of the thermohaline circulation is also reversed (Fig. 8e). It can be considered as a secondary circulation driven by the forced meridionally averaged zonal circulation, as discussed in Section 5. This secondary circulation is important in maintaining the thermocline at high latitudes, by forming warm, instead of cold, bottom water. Detailed discussion of this secondary circulation, and its implications for two-dimensional latitude/depth models, are presented in the next section.

The effects of wind forcing on the thermocline structure can be clearly seen in Figures 8(a)–(c). The thermocline has less bowl-shaped curvature in the low latitudes and is shallower in the buoyancy only case (c), compared to the control case

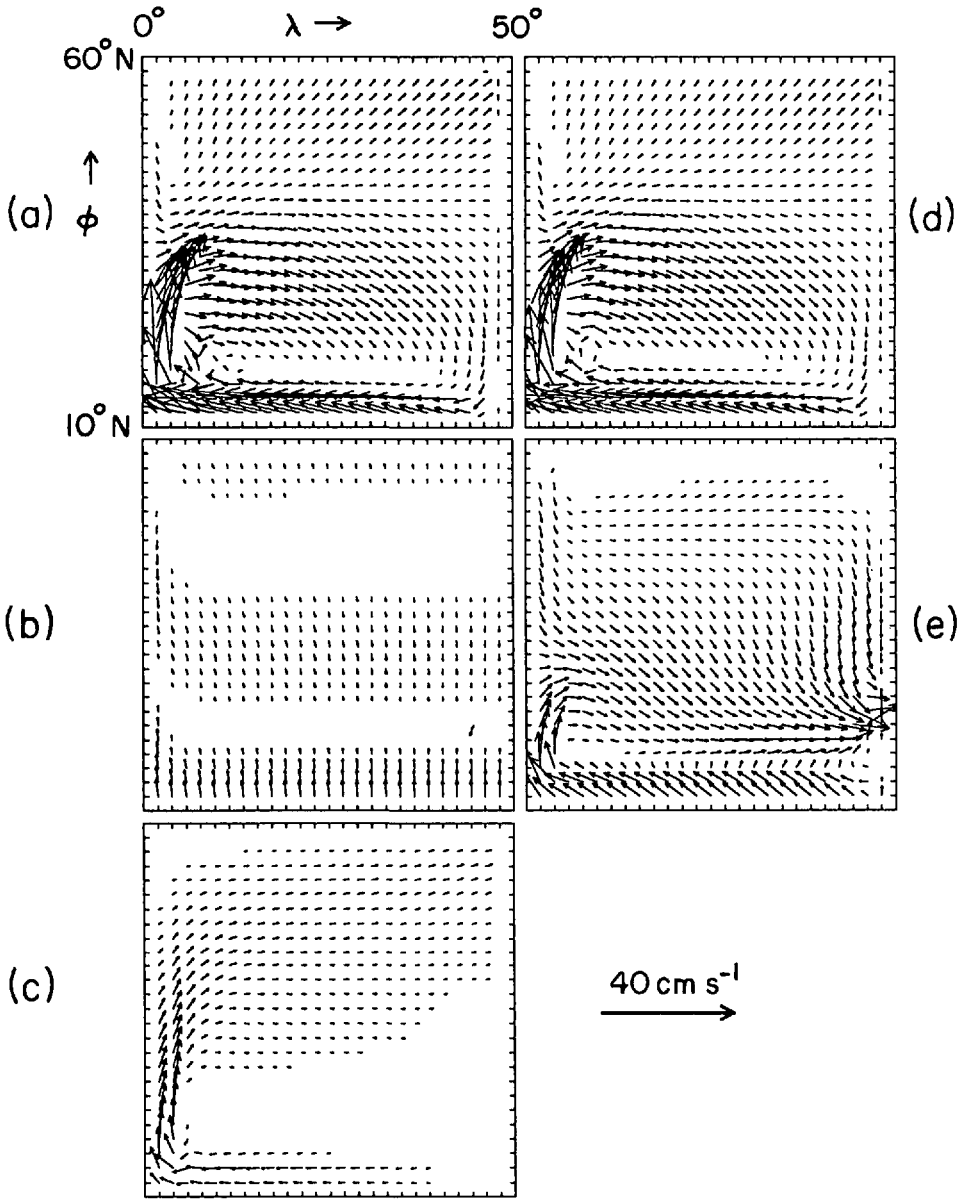

Figure 9. The horizontal circulation (m s^{-1}) at the top model level centered at a depth of 34 m, for cases (a) to (e) of Table 3.

(a). The curvature is due to wind driven upwelling/downwelling, as shown in the wind only case (b). In the latter case, the bowl-shaped distribution is clearly evident, and the thermocline is much deeper, with weak wind-driven overturning cells extending to the ocean bottom. This deep thermocline cannot be sustained when

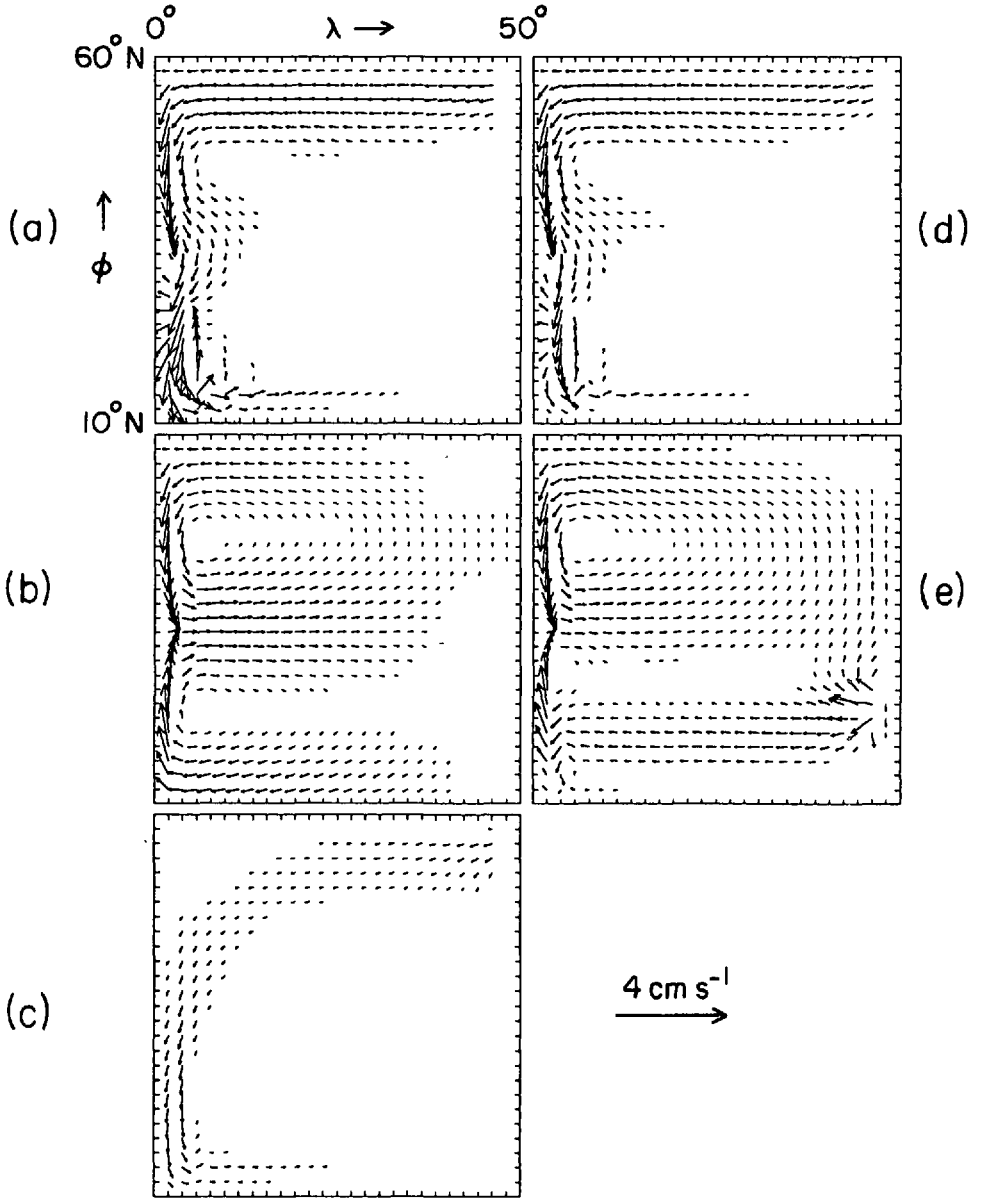

Figure 10. As Figure 9, but for the eighth model level centered at a depth of 2076 m.

baroclinic pressure gradients are present, i.e., cases (a) and (c) with $\epsilon_2 \neq 0$. In these cases, the thermohaline circulation transports cold bottom water below the thermocline, thus providing a source of cold, dense water at depth. This explains why the thermocline in cases (a) and (c) is shallower than in case (b).

Comparing cases (a), (b) and (c), it is clear that buoyancy effects play the dominant role. Many features of case (a), such as the basic thermocline structure and

thermohaline circulation, a strong northward surface current on the western boundary, and a return western boundary current at lower levels, are also features found in case (c), for which the circulation is similar to that originally proposed by Stommel (1958).

In case (d), a damping term is included in the baroclinic momentum equation. This leads to a smoother and weaker motion field, with the velocities being reduced by about 14%. The frictional cross isobaric flow reduces the horizontal pressure gradient. Doubling the dissipative coefficient (γ) in the baroclinic part further reduces the velocity field by about 10%, while a doubling of the coefficient in the barotropic part has negligible effect. The total motion field is however primarily baroclinic; for example, the barotropic velocity contributes only about 10% in the top layer of the subtropical gyre in the control run. Including dissipation in the baroclinic part also leads to a shallower thermocline. The reason seems to be the enhanced vertical motion due to friction. The additional divergence due to frictional dissipation can be estimated as $-(\gamma/f)\zeta$, with ζ being the vorticity, if the less important term due to the β-effect is neglected. This divergence results in upwelling in the anticyclonic subtropical gyre and an upward displacement of the thermocline, as shown by Figures 8(a) and (d).

The above results suggest that the thermocline distribution at low and mid-latitudes is maintained solely by convective overturning, with the thermohaline circulation contributing to its thickness. The thermocline structures remain qualitatively unchanged, aside from the thermocline thickness, for all the cases with convection, (a)–(d). Its structure is changed dramatically when convection is removed in case (e).

Our results in Section 3 suggest that for the same value of the vertical diffusivity, the thermocline in our model is shallower than that of primitive equation models. A shallower thermocline is also simulated by the Hamburg ocean model (Maier-Reimer and Hasselmann, 1987). These are desirable features, as primitive equation models seem to simulate too deep a thermocline and a weak thermohaline circulation (Bryan and Komro, 1984). The reason seems to be a stronger meridional overturning circulation in our model. One possible cause might be the different finite difference scheme used; this seems unlikely as quite different schemes are used in our model (C-grid) and the Hamburg model (E-grid). At steady state, the local time derivative vanishes in both the primitive equation and PG models, so the only remaining effect is the omission of the nonlinear momentum and horizontal viscous terms in the PG system. The latter term is almost certainly more important. We will not, however, attempt to further explore this difference here.

5. The role of convective overturning and implications for 2-D zonally-averaged models

We saw in the previous section that when convective overturning is removed, a thermocline forms at the high latitudes instead of at the low latitudes. The sense of

the thermohaline circulation also reverses. This reversal is critical for maintaining the thermocline, as it forms warm bottom water at the low latitudes instead of cold bottom water in higher latitudes. Ekman drift is not required in this reversal, but it does extend the reversed thermocline to a lower latitude. We now examine further the role of convection in the formation of the thermocline and thermohaline circulation in the model and discuss the implications of our results for two-dimensional, zonally-averaged models such as Marotzke *et al.* (1988) and Wright and Stocker (1991). In particular, we discuss cases (a) and (e) as shown in Table 3. Recall case (a) is the control run with wind and buoyancy forcings, and convection, while case (e) is the same case but with no convection.

Before examining these cases, we note from Eq. (7) that in the absence of wind forcing ($\tau_s = 0$), the momentum balance is among the Coriolis, pressure gradient, and frictional forces. For two-dimensional latitude/depth models, the treatment of the east-west pressure gradient term is problematic. One way to circumvent this difficulty is to assume a frictional balance between the frictional and pressure gradient forces (e.g., Marotzke *et al.,* 1988). This is formally equivalent to considering a narrow ocean basin for which the influence of rotation on the cross-channel flow can be neglected. (An alternative treatment, not relying on the "narrow basin" approximation, is given by Wright and Stocker (1991); this also leads to an equation similar to (12) below.) The meridional momentum equation can then be written

$$-\gamma v' = \rho^{-1} p'_y \tag{9}$$

where $p' = p - p^+$ is the baroclinic pressure. On the other hand, the north-south flow is in approximate geostrophic balance, so that

$$fv' = \rho^{-1} p'_x. \tag{10}$$

Eqs. (9) and (10) are equivalent in the zonally averaged form if the following holds.

$$-f\,[p']_y = \gamma(p'_E - p'_W)/\Delta x. \tag{11}$$

Here, square brackets denote a zonal average over the extent Δx, and subscripts E and W denote values at the eastern and western sides of the basin respectively. Eq. (11) thus implies a certain slope of the isobars on a horizontal plane.

$$(\partial y/\partial x)_p = -p'_x/p'_y = f/\gamma. \tag{12}$$

A constraint of this kind where the east-west pressure difference is related to the north-south gradient is in general satisfied (Wright and Stocker, 1991); this may be the reason why two-dimensional models are successful at reproducing many results from three-dimensional models (e.g., Marotzke *et al.,* 1988; Stocker and Wright, 1991). However, we will show that in the case (e) when convective adjustment is removed in our model, the reversal of the sign of the east-west pressure gradient means that this constraint no longer holds. This means that experiments using

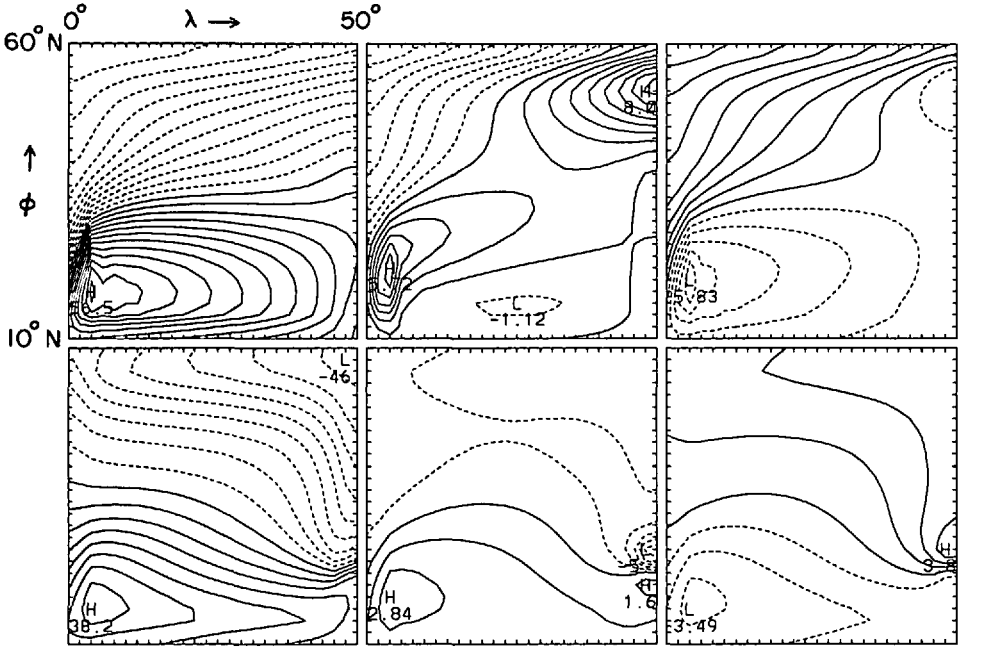

Figure 11. The horizontal distribution of the baroclinic pressure fields, in units of 100 N m^{-2}, at vertical levels 1, 5, and 9. The top panels are for the control case (a) of Table 3, while the bottom panels are for the case (e) without convective overturning.

zonally averaged models in which the convective overturning is suppressed (e.g., Marotzke *et al.,* 1988) are not valid.

The zonally averaged pressure distributions (not shown) for the control case (a) and case (e) are quite similar, despite the reversed thermohaline circulation of the latter case. This is because of the strong constraint imposed by the surface forcing. Due to this forcing, the high latitudes are cold with a lower baroclinic pressure; the north-south pressure gradient thus remains qualitatively the same in the two cases. According to the frictional balance expressed by Eq. (9), this pressure gradient would result in a thermohaline circulation with cold water sinking at high latitudes, as in the control simulation. The bottom water thus created also maintains the thermocline shape similar to that in the control case. This is the reason why the two-dimensional results remain qualitatively identical when convection is removed (e.g., Marotzke *et al.,* 1988). However, the results are totally modified for the case (e) with no convection in our three-dimensional model.

We show in Figure 11 the baroclinic pressure fields at levels 1, 5 and 9, for cases (a) and (e). These are obtained by vertical integration of the hydrostatic equation, with the integration constant determined by the requirement that the vertical mean be zero. The velocity fields at levels 1 and 8 have already been examined in Figures 9 and 10. As noted earlier, the sense of the north-south pressure gradient remains the same

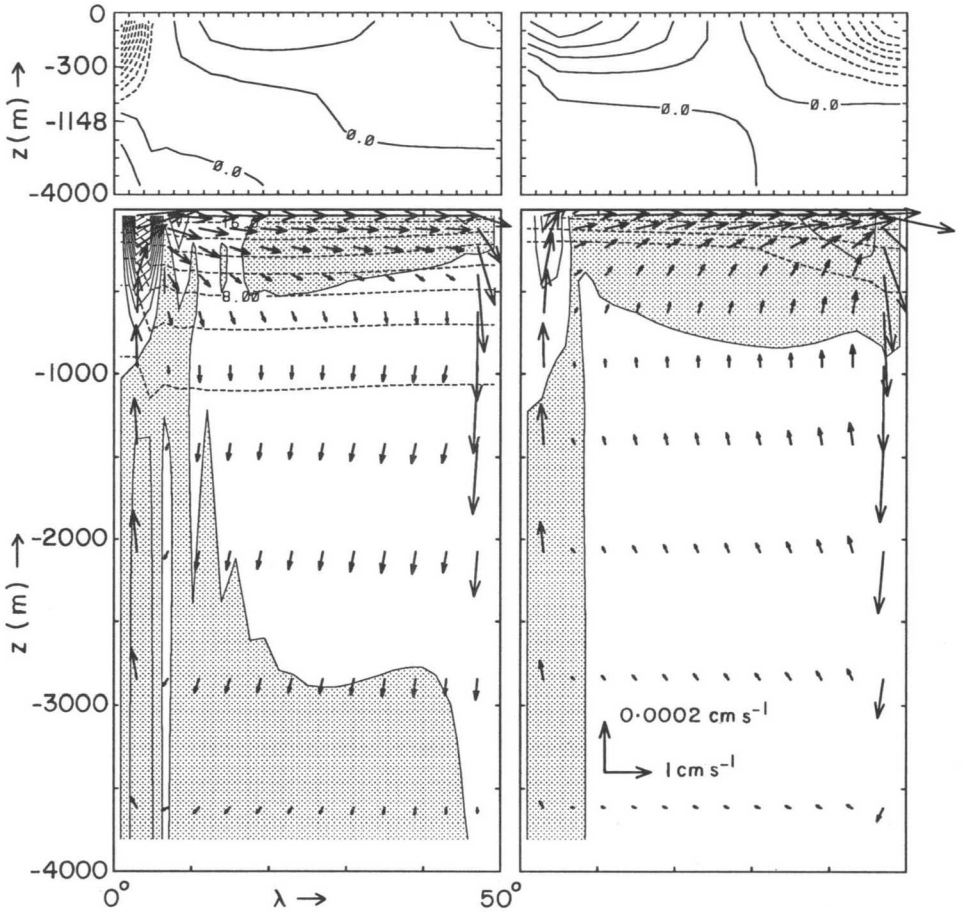

Figure 12. The basin wide meridionally averaged sections for cases (a) (left panels) and (e) (right panels) of Table 3. The bottom panels show the isotherms (°C, dashed lines), the (u, w) velocity vectors, and the meridional velocity component (v contour interval is 1 cm s^{-1}, shading indicates negative values and is to the south). The top panels show the baroclinic pressure field, with a contour interval of 200 N m^{-2}.

in the two cases, due to the unchanged surface forcing. However, the sense of the east-west pressure gradient, as revealed by the horizontal slope of the isobars in Figure 11, is reversed in case (e). The southwest-northeast tilt in case (a) is changed to a northwest-southeast tilt in case (e). This means that Eq. (11) is not satisfied in the latter case. Frictional effects can turn the velocity toward lower pressure (i.e., high latitudes), but unrealistically strong friction is needed to reverse back the sense of the tilt of case (e).

Figure 12 shows the meridionally averaged distributions of temperature, pressure, meridional velocity, and zonal circulation, for the two cases. Through thermal wind

balance, the forced north-south surface pressure gradient leads to a meridionally averaged west to east surface flow in both cases, resulting in upwelling in the western part of the basin, and downwelling in the eastern part. These vertical motions advect bottom water upward in the west, and surface waters downward in the east. However, because bottom water is formed at different locations in the two cases (Fig. 8), the bottom water is denser relative to the surface water in case (a), and lighter in case (e). This vertical water mass distribution results in a reversed east-west surface pressure gradient for case (e) in Figures 11 and 12, which in turn leads to a reversed zonally averaged thermohaline circulation on the vertical plane, as shown already in Figure 8. The meridional overturning circulation can thus be regarded as a secondary circulation satisfying geostrophic balance as expressed by (10); it is secondary as the east-west surface pressure gradient is not directly constrained by the surface forcing. On the other hand, the zonal overturning circulation is directly forced by the north-south surface pressure gradient, and thus may be termed the primary circulation. The sense of the secondary circulation is determined by the vertical distribution of water mass. In case (a), it is toward the north at the surface when lighter water is on top; while it is southward when denser water is on top, as in case (e) with convective adjustment suppressed.

We noted at the end of Section 3 that as the vertical diffusivity is increased, the thermocline depth increases and so does the strength of the meridional overturning circulation. The connection between the thermocline depth and the strength of the meridional overturning circulation can be understood in terms of the mechanism of the secondary circulation described above. Recall the baroclinic horizontal pressure gradient is determined by the vertical integration of the horizontal density gradient. The north-south density gradient at the surface is forced and cannot vary much. As the thermocline depth increases, this density gradient extends to greater depths leading to an enhanced north-south pressure gradient and a stronger east-west primary circulation. This drives the secondary, meridional overturning circulation, as described above. In particular, the east-west pressure difference is again determined by the isopycnal displacements due to advection by the primary east-west circulation. The deeper the thermocline the stronger the east-west pressure difference and hence the stronger the meridional overturning circulation. The wind stress and vertical diffusivity can increase the depth of the thermocline; this explains the sensitivity of the overturning circulation to these parameters found in Bryan and Cox (1967), Cox and Bryan (1984), Bryan (1987), as well as in our study.

6. Conclusions

We have formulated a multi-level spherical model using the planetary geostrophic (PG) system of equations. The PG system takes advantage of the large scale separation in the ocean between the internal Rossby radius of deformation and the basin scale. The use of the PG system means that the time step is limited only by the

ocean current speed. This leads to a computationally efficient model, compared to primitive equation models, without the need to use asynchronous integration techniques (e.g., Bryan (1984)).

Comparison of the PG to primitive equation (PE) model results show that PG dynamics is capable of reproducing many of the features (thermocline structure, meridional streamfunction, tracer and potential vorticity distributions) of primitive equation models. With a larger value of the vertical diffusivity and coarser horizontal resolution than PE models, the PG model simulates a thermocline of comparable depth, as well as velocities on the meridional plane of comparable magnitudes. The need to use a larger vertical diffusivity is attributed to the large horizontal eddy viscosity in PE models, which is absent in the PG model. Both models show a similar sensitivity to the value of the vertical diffusivity.

Additional numerical experiments have been performed in order to determine the major processes that determine the model circulation. An interesting result is the crucial role of convective overturning in maintaining the thermocline distribution by providing a source of cold, dense water at depth. Removal of convective overturning dramatically alters the circulation in the model, as the thermohaline circulation reverses direction and a hydrostatically unstable thermocline develops at high latitudes. Through geostrophy, the sense of the former is determined by the east-west pressure gradient, which in turn is determined by the water mass distribution. In particular, we have shown how the sign of the east-west pressure gradient is reversed in the presence of a hydrostatically unstable thermocline, leading to the reversed thermohaline circulation. This is unlike two-dimensional zonally averaged models, where the east-west gradient is constrained by the north-south gradient. The latter is in turn determined by the surface forcing and is essentially the same whether convective overturning is included or not. This means results of experiments with two-dimensional models where convective overturning is suppressed are not valid.

Finally, we note that the use of a long time step with the PG model means that it is ideally suited for ocean-climate studies. Problems such as interannual variability and the effect of seasonally varying forcing can be addressed using our model without the use of asynchronous time stepping methods.

Acknowledgments. This work forms part of the Canadian university participation in the World Ocean Circulation Experiment (WOCE), and is supported by the Collaborative Research Initiatives Program of the Natural Sciences and Engineering Research Council (NSERC) of Canada. We wish to thank Dr. A. Weaver, the two reviewers and Dr. G. Veronis for helpful comments. We are also grateful to Ursula Seidenfuss for drafting the figures and to Joy Simmons for assistance with the typing at the revision stage.

REFERENCES

Bacastow, R. and E. Maier-Reimer. 1990. Ocean-circulation model of the carbon cycle. Climate Dyn., *4,* 95–125.

Bryan, F. 1987. Parameter sensitivity of primitive equation ocean general circulation models. J. Phys. Oceanogr., *17,* 970–985.

Bryan, K. 1969. A numerical method for the study of the circulation of the world ocean. J. Comput. Phys., *4,* 347–376.

—— 1984. Accelerating the convergence to equilibrium of ocean-climate models. J. Phys. Oceanogr., *14,* 666–673.

Bryan, K. and M. D. Cox. 1967. A numerical investigation of the oceanic general circulation. Tellus, *19,* 54–80.

—— 1972. An approximate equation of state for numerical models of ocean circulation. J. Phys. Oceanogr., *2,* 510–514.

Bryan, K. and F. G. Komro. 1984. The ocean's transient response to global surface temperature anomalies, *in* Climate Processes and Climate Sensitivity, J. E. Hansen and T. Takahashi, eds., Amer. Geophys. Union, Washington, D.C., 368 pp.

Bryan, K. and L. J. Lewis. 1979. A water mass model of the world ocean. J. Geophys. Res., *84,* 2503–2517.

Colin de Verdière, A. 1988. Buoyancy driven planetary flows. J. Mar. Res., *46,* 215–265.

—— 1989. On the interaction of wind and buoyancy driven gyres. J. Mar. Res., *47,* 595–633.

Cox, M. D. 1984. A primitive equation, three-dimensional model of the ocean. GFDL Ocean Group Tech. Rep. No. 1.

—— 1985. An eddy resolving numerical model of the ventilated thermocline. J. Phys. Oceanogr., *15,* 1312–1324.

Cox, M. D. and K. Bryan. 1984. A numerical model of the ventilated thermocline. J. Phys. Oceanogr., *14,* 674–687.

Greatbatch, R. J. and A. Goulding. 1992. A long-time-scale, density-stratified shelf circulation model. Cont. Shelf Res., *12,* 115–142.

Haney, R. L. 1971. Surface thermal boundary condition for ocean circulation models. J. Phys. Oceanogr., *1,* 241–248.

Hasselmann, K. 1982. An ocean model for climate variability studies. Prog. Oceanogr., *11,* 69–92.

Killworth, P. D. 1983. Some thoughts on the thermocline equations. Ocean Modelling, No. 48, (unpublished manuscript).

—— 1985. A two-level wind and buoyancy driven thermocline model. J. Phys. Oceanogr., *15,* 1414–1432.

Luyten, J. R., J. Pedlosky and H. M. Stommel. 1983. The ventilated thermocline. J. Phys. Oceanogr., *13,* 292–309.

Maier-Reimer, E. and K. Hasselmann. 1987. Transport and storage of CO_2 in the ocean—An inorganic ocean circulation carbon cycle model. Climate Dyn., *2,* 63–90.

Marotzke, J., P. Welander and J. Willebrand. 1988. Instability and multiple steady states in a meridional-plane model of the thermohaline circulation. Tellus, *40A,* 162–172.

Robinson, A. R. and H. Stommel. 1959. The oceanic thermocline and the associated thermocline circulation. Tellus, *3,* 295–308.

Salmon, R. 1986. A simplified linear ocean circulation theory. J. Mar. Res., *44,* 695–711.

—— 1990. The thermocline as an internal boundary layer. J. Mar. Res., *48,* 437–469.

Stocker, T. F. and D. G. Wright. 1991. A zonally averaged ocean model for the thermohaline circulation. Part II: Interocean circulation in the Pacific-Atlantic basin systems. J. Phys. Oceanogr., *21,* 1725–1739.

Stommel, H. 1948. The westward intensification of wind-driven ocean currents. Trans. Amer. Geophys. Union, *29,* 202–206.

—— 1958. The abyssal circulation. Deep-Sea Res., *5,* 80–82.

Veronis, G. 1973. Models of World Ocean Circulation: 1. Wind-driven, two-layer. J. Mar. Res., *31,* 228–289.

Weaver, A. J. and E. S. Sarachik. 1989. On the importance of vertical resolution in certain ocean general circulation models. J. Phys. Oceanogr., *20,* 600–609.

—— 1991. The role of mixed boundary conditions in numerical models of the ocean's climate. J. Phys. Oceanogr., *21,* 1470–1493.

Wright, D. G. and T. F. Stocker. 1991. A zonally averaged ocean model for the thermohaline circulation. Part I: Model development and flow dynamics. J. Phys. Oceanogr., *21,* 1713–1724.

Received: *3 September, 1991;* revised: *17 December, 1991*